
NEURAL DIFFUSION PROCESSES

A PREPRINT

Vincent Dutordoir
University of Cambridge
Secondmind

Alan Saul
Secondmind

Zoubin Ghahramani
University of Cambridge
Google Research, Brain Team

Fergus Simpson
Secondmind

ABSTRACT

Gaussian processes provide an elegant framework for specifying prior and posterior distributions over functions. They are, however, also computationally expensive, and limited by the expressivity of their covariance function. We propose Neural Diffusion Processes (NDPs), a novel approach based upon diffusion models, that learns to sample from distributions over functions. Using a novel attention block we are able to incorporate properties of stochastic processes, such as exchangeability, directly into the NDP’s architecture. We empirically show that NDPs are able to capture functional distributions that are close to the true Bayesian posterior of a Gaussian process. This enables a variety of downstream tasks, including hyperparameter marginalisation and Bayesian optimisation.

1 Introduction

Gaussian processes (GPs) offer a powerful framework for defining distributions over functions [23]. A key benefit of GPs is their exchangeability, which makes it possible to get consistent predictions at arbitrary locations from a trained model. However, two key factors limit the scope of real-world tasks that can be effectively tackled with GPs. Firstly, the cost of inference scales as $\mathcal{O}(N^3)$, where N is the number of datapoints. Secondly, the conventional approach of adopting a point estimate for the hyperparameters is often problematic, while the more principled solution of performing full marginalisation can be prohibitively computationally expensive [13].

Neural network (NN) based generative models can also learn a distribution over functions, allowing them to mimic GPs. Successful methods include the meta-learning approaches of Neural Processes (NPs) [8], the Gaussian NPs [2, 18], and the VAE-based [19, 6]. By leveraging a large number of small datasets during training, they are able to transfer knowledge across datasets at prediction time. Using NNs is appealing since most of the computational effort is expended during the training process, while the task of prediction becomes usually considerably more straightforward. A further major advantage of a NN-based approach is that it allows full marginalisation over the GP hyperparameters, a task that can prove computationally challenging for conventional GP models, even for relatively small datasets.

We seek to improve on these methods by extending an existing state-of-the-art NN-based generative model. In terms of sample quality, the so-called probabilistic denoising diffusion model [27, 28, 9] has recently been shown to outperform existing generative methods on tasks such as image [20, 22], molecular structure [34], point cloud [17] and audio signal [12] generation. However, out-of-the-box diffusion models are not able to generate samples from continuous stochastic processes. This is difficult, because we require the samples to be *functions* that can be evaluated at arbitrary locations in their input domain. Additionally for the samples to be drawn from a stochastic process, we expect them to adhere to certain properties, such as exchangeability — i.e., the joint probability distribution does not change when the order of function evaluations is altered. This makes the problem fundamentally different from generating images, or audio waves.

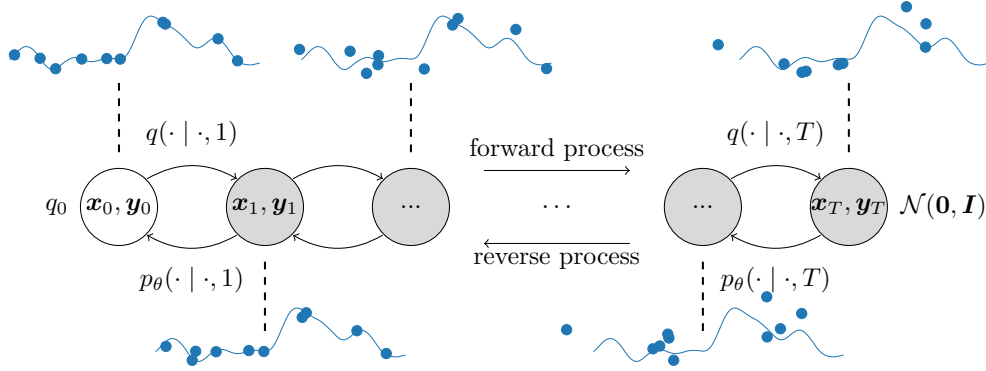


Figure 1: Illustration of the **forward and reverse process** of NDPs. (Left-to-right) During the forward process, data points (blue dots) from a function draw (blue line) are perturbed by increasing levels of noise until the points (both inputs and output values) are given by white noise. (Right-to-left) The reverse process consists of gradually removing noise until we arrive at a data point.

Contributions We propose a novel model, the Neural Diffusion Process (NDP), which extends the use case of diffusion models to stochastic processes and is able to describe a rich distribution over functions. NDPs generalise diffusion models to infinite-dimensional function spaces by allowing the indexing of random variables onto which the model diffuses. We take particular care to enforce known symmetries and properties of a stochastic processes, including exchangeability, into the model, facilitating the training process. These properties are enforced with the help of a novel attention component, namely the *bi-dimensional* attention block, which guarantees equivariance over the (1) input dimensionality and (2) the sequence (i.e., datapoints) ordering. We showcase the abilities and versatility of NDPs by applying them to a range of Bayesian inference tasks including prior and conditional sampling, regression, hyperparameter marginalisation, and Bayesian optimisation. We also present a novel global optimisation method using NDPs.

2 Denoising Diffusion Probabilistic Models for Stochastic Processes

Diffusion models [9, 27, 28] have the ability to create high-quality samples from complex, high-dimensional distributions. So far, the literature has predominantly focused on generating samples from distributions in one, two and three dimensions (such as audio, images, point clouds and molecules). Furthermore, the feature being generated in all of these examples is either a varying output on a predefined input or a fixed output with a varying input location. For example, in image generation we assume a predefined configuration of pixels. In audio synthesis, the random variables are ordered according to a discretisation of the real line. NDPs generalise diffusion models to infinite-dimensional function spaces by allowing function observations \mathbf{y} to be indexed by another set of random variables \mathbf{x} . At prediction, this makes it possible to evaluate the NDP’s function samples anywhere in their input domain. This allows stochastic processes, such as GPs, to be modelled.

Diffusion models operate using two components: a *forward* and a *reverse* process, as illustrated in fig. 1. The forward process consists of a Markov chain, which incrementally adds random noise to the data. The reverse process is tasked with inverting this chain in order to construct desired data samples from noise. In order to accurately approximate the complex reverse process, in section 3 we will introduce a novel neural network architecture for the NDP and discuss how it hard-wires known symmetries and properties of a stochastic processes (e.g., exchangeability) into its architecture. First, we will extend the vanilla diffusion model components to accommodate the sampling of functions.

Notation Let $[\mathbf{a}]_i$ select the i -th element of a column vector. Let $f : \mathcal{X} \rightarrow \mathbb{R}$ be a function, $\mathbf{y} \in \mathbb{R}^N$ a vector of N noisy function evaluations, and $\mathbf{x} \in \mathcal{X}^N$ a vector of N inputs that adhere to the relationship: $[\mathbf{y}]_i = f([\mathbf{x}]_i) + \eta$, where $\eta \sim \mathcal{N}(0, \sigma^2)$ corresponds to the observation noise.

Forward process For NDPs, the data distribution $(\mathbf{x}_0, \mathbf{y}_0) \sim q(\mathbf{x}_0, \mathbf{y}_0)$ consists of samples of stochastic processes. We construct it by defining a prior distribution over input locations $q(\mathbf{x}_0)$,

and a prior over observations $q(\mathbf{y}_0 \mid \mathbf{x}_0)$ conditioned on the inputs. Samples from these priors will be used as training datasets. For the inputs, we choose them to be drawn i.i.d. from a uniform measure over the input domain, whereas the prior over observations is chosen to be a centred GP $q(\mathbf{y}_0 \mid \mathbf{x}_0) = \mathcal{N}(\mathbf{y}_0; \mathbf{0}, k_\psi(\mathbf{x}_0, \mathbf{x}_0) + \sigma^2 \mathbf{I})$, with a covariance function k_ψ with hyperparameters ψ . Let us then define the forward process as a fixed Markov chain, which iteratively corrupts $(\mathbf{x}_0, \mathbf{y}_0)$ by adding small amounts of noise at each step

$$q(\mathbf{y}_{0:T}, \mathbf{x}_{0:T}) = q(\mathbf{x}_0) q(\mathbf{y}_0 \mid \mathbf{x}_0) \prod_{t=1}^T q\left(\begin{bmatrix} \mathbf{x}_t \\ \mathbf{y}_t \end{bmatrix} \mid \begin{bmatrix} \mathbf{x}_{t-1} \\ \mathbf{y}_{t-1} \end{bmatrix}, t\right), \quad (1)$$

where the corrupting distribution $q(\cdot \mid \cdot, t)$ is jointly Gaussian

$$q\left(\begin{bmatrix} \mathbf{x}_t \\ \mathbf{y}_t \end{bmatrix} \mid \begin{bmatrix} \mathbf{x}_{t-1} \\ \mathbf{y}_{t-1} \end{bmatrix}, t\right) = \mathcal{N}\left(\begin{bmatrix} \mathbf{x}_t \\ \mathbf{y}_t \end{bmatrix} \mid \sqrt{1 - \beta_t} \begin{bmatrix} \mathbf{x}_{t-1} \\ \mathbf{y}_{t-1} \end{bmatrix}, \beta_t \mathbf{I}\right). \quad (2)$$

The size of the noise in each step is controlled by a pre-specified variance schedule $\{\beta_t \in (0, 1)\}_{t=1}^T$. Note that there is no learning involved in the forward process it simply creates a sequence of random variables $\{(\mathbf{x}_t, \mathbf{y}_t)\}_{t=1}^T$ which progressively look more like white noise as t approaches T , as shown in fig. 1.

A useful property of the forward process, thanks to the linearity of Gaussians, is that we can bypass the iterative forward generation and directly sample at any arbitrary time step $t \in \{1, 2, \dots, T\}$. Let $\gamma_t = \sqrt{1 - \bar{\alpha}_t}$ and $\bar{\alpha}_t = \prod_{j=1}^t (1 - \beta_j)$. Then, by relying on the reparameterisation trick \mathbf{x}_t and \mathbf{y}_t can be sampled using

$$\mathbf{x}_t = \sqrt{\bar{\alpha}_t} \mathbf{x}_0 + \gamma_t \boldsymbol{\varepsilon}_x \quad \text{and} \quad \mathbf{y}_t = \sqrt{\bar{\alpha}_t} \mathbf{y}_0 + \gamma_t \boldsymbol{\varepsilon}_y, \quad (3)$$

where $\boldsymbol{\varepsilon}_x, \boldsymbol{\varepsilon}_y \sim \mathcal{N}(\mathbf{0}, \mathbf{I})$.

Reverse process The goal of the reverse process is the creation of target data (i.e., function draws) starting from white noise at time T . While the forward process is designed to be Markovian, the true reverse probability requires the entire sequence. Let us define an approximation to this reverse process as

$$p_\theta(\mathbf{x}_{0:T}, \mathbf{y}_{0:T}) = p(\mathbf{x}_T, \mathbf{y}_T) \prod_{t=1}^T p_\theta\left(\begin{bmatrix} \mathbf{x}_{t-1} \\ \mathbf{y}_{t-1} \end{bmatrix} \mid \begin{bmatrix} \mathbf{x}_t \\ \mathbf{y}_t \end{bmatrix}, t\right),$$

which starts from a white noise initial state $p(\mathbf{x}_T, \mathbf{y}_T) = \mathcal{N}(\mathbf{0}, \mathbf{I})$ and where p_θ is a *parameterised* backward Markov kernel. The backward kernel is tasked with learning to reverse each step in eq. (1), which is a complicated function that depends on the inputs, $\mathbf{x}_t, \mathbf{y}_t$ as well as the time. Following Ho et al. [9], we parameterise p_θ as a Gaussian, where the mean is constructed using parameterised outputs $\boldsymbol{\epsilon}_\theta^x(\cdot)$ and $\boldsymbol{\epsilon}_\theta^y(\cdot)$ from the current state:

$$p_\theta\left(\begin{bmatrix} \mathbf{x}_{t-1} \\ \mathbf{y}_{t-1} \end{bmatrix} \mid \begin{bmatrix} \mathbf{x}_t \\ \mathbf{y}_t \end{bmatrix}, t\right) = \mathcal{N}\left(\begin{bmatrix} \mathbf{x}_{t-1} \\ \mathbf{y}_{t-1} \end{bmatrix} \mid \frac{1}{\sqrt{1 - \beta_t}} \left(\begin{bmatrix} \mathbf{x}_t \\ \mathbf{y}_t \end{bmatrix} - \frac{\beta_t}{\gamma_t} \begin{bmatrix} \boldsymbol{\epsilon}_\theta^x(\mathbf{x}_t, \mathbf{y}_t, t) \\ \boldsymbol{\epsilon}_\theta^y(\mathbf{x}_t, \mathbf{y}_t, t) \end{bmatrix}\right), \frac{\gamma_t^2}{\gamma_{t-1}^2} \beta_t \mathbf{I}\right). \quad (4)$$

In what comes next we refer to $\boldsymbol{\epsilon}_\theta^x(\cdot)$ and $\boldsymbol{\epsilon}_\theta^y(\cdot)$ as noise models, as they are effectively learning to predict the noise that was added to the true data points, so that it can be removed for each backwards step in the reverse process. In section 3 we discuss their design such that the reverse process gives rise to function draws that adhere to the properties of stochastic processes. For the remainder of this section, we assume they are given but that they have a set of parameters θ that require optimisation.

The parameters θ of the noise models $\boldsymbol{\epsilon}_\theta^x(\cdot)$ and $\boldsymbol{\epsilon}_\theta^y(\cdot)$ can be trained by optimising a variational lower bound to the model evidence $\log p_\theta(\mathbf{x}_0, \mathbf{y}_0)$. However, following Kingma et al. [11], NDPs use a re-weighted variational lower bound where the weighting is chosen for the purposes of sample quality and easier optimisation (see appendix A for a detailed derivation), which gives

$$\mathcal{L}_\theta = \mathbb{E}_{\mathbf{x}_0, \mathbf{y}_0, \boldsymbol{\varepsilon}_x, \boldsymbol{\varepsilon}_y, t} \left[\|\boldsymbol{\varepsilon}_x - \boldsymbol{\epsilon}_\theta^x(\mathbf{x}_t, \mathbf{y}_t, t)\|^2 + \|\boldsymbol{\varepsilon}_y - \boldsymbol{\epsilon}_\theta^y(\mathbf{x}_t, \mathbf{y}_t, t)\|^2 \right]. \quad (5)$$

We can obtain stochastic estimates of \mathcal{L}_θ by sampling $\mathbf{x}_0 \sim q(\mathbf{x}_0)$, $\mathbf{y}_0 \sim q(\mathbf{y}_0 \mid \mathbf{x}_0)$, $\boldsymbol{\varepsilon}_x, \boldsymbol{\varepsilon}_y \sim \mathcal{N}(\mathbf{0}, \mathbf{I})$, and $t \sim \mathcal{U}(\{1, 2, \dots, T\})$. Note that $\mathbf{x}_t = \sqrt{\bar{\alpha}_t} \mathbf{x}_0 + \gamma_t \boldsymbol{\varepsilon}_x$ and $\mathbf{y}_t = \sqrt{\bar{\alpha}_t} \mathbf{y}_0 + \gamma_t \boldsymbol{\varepsilon}_y$ are created using eq. (3). From the objective, it becomes clear that the noise models $\boldsymbol{\epsilon}_\theta^x(\cdot)$, $\boldsymbol{\epsilon}_\theta^y(\cdot)$ are trained to predict the noise $\boldsymbol{\varepsilon}_x, \boldsymbol{\varepsilon}_y$ that was added to the true data points. The question still remains as to what parameterised models should be used for $\boldsymbol{\epsilon}_\theta^x(\cdot)$ and $\boldsymbol{\epsilon}_\theta^y(\cdot)$; we defer our answer to section 3 whilst we discuss details of how coherent samples can be obtained under the assumption of an accurate approximate noise model.

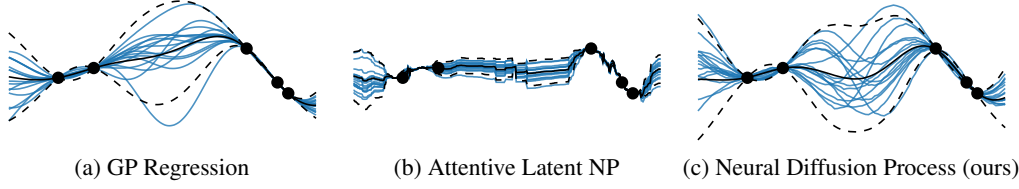


Figure 2: **Conditional samples:** The blue curves are posterior samples conditioned on the context dataset (black dots) from different probabilistic models. We also plot the empirical mean and two standard deviations of the samples in black. More examples are given in fig. D.1

2.1 Inference and Conditional samples

So far we have shown how NDPs are able to generate prior function draws by traversing the reverse process using the backward kernel p_θ . In this section, we detail how NDPs are able to draw *conditional* samples from the posterior $p(x_0, y_0 \mid \mathcal{D})$ where $\mathcal{D} = \{([x_0^c]_i \in \mathcal{X}, [y_0^c]_i \in \mathbb{R})\}_{i=1}^n$ is the *context* dataset. This is analogous to how we draw posterior samples from a GP conditioned on a dataset \mathcal{D} , as shown in fig. 2a. For notational simplicity, we present the sampling scheme for a single input and corresponding output (x_0, y_0) , but we stress that all the operations can be batched to obtain M correlated inputs and corresponding outputs originating from the same function draw.

Following recent advances in image in-painting with diffusion models [16], we adjust the reverse process to account for the information in \mathcal{D} . We want the conditional samples to be correlated and consistent with the context dataset. The conditional sampling process works as follows: We start by augmenting the intermediate state to contain information about the context dataset in (x_t^c, y_t^c) , and about the initial random state in (x_t, y_t) . This results in the augmented intermediate state $\mathbf{x}_t = [x_t^c, x_t]$ and $\mathbf{y}_t = [y_t^c, y_t]$. The part of intermediate state that correspond to context points (x_t^c, y_t^c) is created by using the forward process starting from the context data (x_0^c, y_0^c) (left hand side of eq. (6)), while (x_t, y_t) is created using the backward kernel (right hand side) starting from the initial states at $t = T$, $x_T \sim \mathcal{N}(\mathbf{0}, \mathbf{I})$ and $y_T \sim \mathcal{N}(0, 1)$:

$$\begin{aligned} \begin{bmatrix} x_t^c \\ y_t^c \end{bmatrix} &\sim \mathcal{N}\left(\begin{bmatrix} x_0^c \\ y_0^c \end{bmatrix} \mid \sqrt{\alpha_t} \begin{bmatrix} x_0^c \\ y_0^c \end{bmatrix}, \gamma_t^2 \mathbf{I}_n\right) & \text{ and } & \begin{bmatrix} x_t \\ y_t \end{bmatrix} &\sim p_\theta\left(\begin{bmatrix} x_t \\ y_t \end{bmatrix} \mid \begin{bmatrix} x_{t+1} \\ y_{t+1} \end{bmatrix}, t+1\right). \end{aligned} \quad (6)$$

t forward steps (eq. (3)) backward step (eq. (4))

This scheme makes sure that for each backward step (RHS of eq. (6)) we leverage the context dataset as it is contained in the augmented state $(\mathbf{x}_t, \mathbf{y}_t)$. We give examples of this process in fig. 2c and fig. 5 in resp. 1D and 2D, and pseudocode in appendix B.

Note that drawing conditional samples requires only a pretrained *unconditional* NDP. During training NDPs are only concerned with learning the prior. There is no inconvenient target/context dataset split required for creating training examples, as is the case for NPs (e.g. [8, 7, 10]). By design, the same NDP will generalise from zero to an arbitrary number of conditioning points, as shown in fig. 2c.

2.2 Deterministic input locations

In supervised learning the inputs are known in advance, which renders the joint generative distribution $p(x_0, y_0)$ of less importance than the conditional $p(y_0 \mid x_0)$. If this is the use-case of the model, we recommend not to diffuse the inputs, but instead keeping them fixed, i.e. $x_0 = x_1 = \dots = x_T$. Mathematically, this is equivalent to setting ε_x deterministically to zero, which renders its corresponding predictor $\epsilon_\theta^x(\cdot)$ unnecessary and thus reduces eq. (5) to

$$\mathcal{L}_\theta = \mathbb{E}_{\mathbf{x}_0, \mathbf{y}_0, \varepsilon_y, t} \left[\|\varepsilon_y - \epsilon_\theta^y(\mathbf{x}_0, \mathbf{y}_t, t)\|^2 \right]. \quad (7)$$

The noise model $\epsilon_\theta^y(\cdot)$ now acts on the *uncorrupted* inputs \mathbf{x}_0 but still on corrupted observations $\mathbf{y}_t = \sqrt{\alpha_t} \mathbf{y}_0 + \gamma_t \varepsilon_y$. As mentioned, for classic regression tasks it is an unnecessary complexity to diffuse the input locations. However, in section 4 we introduce a novel Bayesian optimisation algorithm which offers an example where having access to the full distribution $p(\mathbf{x}_0, \mathbf{y}_0)$ is critical. Finally, using eq. (7) in training still results in a model of an infinite-dimensional function space prior, which can be evaluated anywhere in its domain \mathcal{X} .

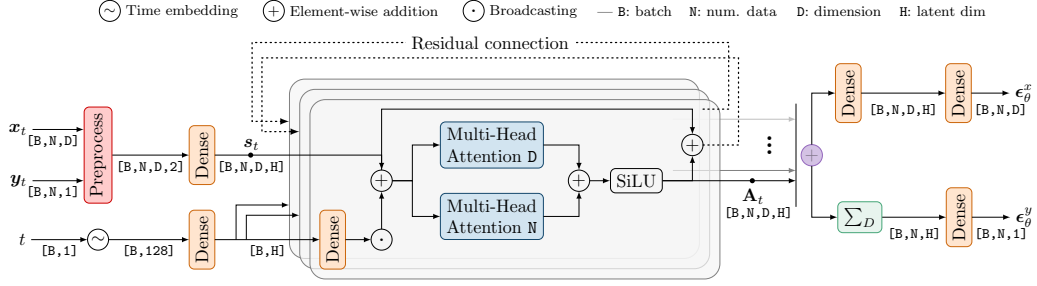


Figure 3: Architecture of the **noise prediction model**, utilised at each step within the Neural Diffusion Process. The greyed box represents the **bi-dimensional** attention block, as discussed in Section 3.2.

3 The noise model and the bi-dimensional attention block

Here, we review the architecture and key components of the NDP’s noise model, including a novel form of attention block in section 3.2. As explained in the previous section, the noise model produces outputs $\epsilon_x(\cdot)$ (resp. $\epsilon_\theta^y(\cdot)$), which attempt to predict the noise ϵ_x (resp. ϵ_y) that needs to be subtracted in order to recover denoised values x_0 from x_t (and resp. y_0 from y_t).

NDPs use a neural network as its noise model. In principle, *any* neural network could be used. However, if we wish for NDPs to mimic GPs, the noise model must learn to generate a prior distribution over functions. In general, we expect such a prior to possess several key symmetries, and these symmetries will heavily influence our choice of architecture. One of the most fundamental properties of stochastic processes, as specified by the Kolmogorov extension theorem, is an *equivariance* to the ordering of inputs. As such, shuffling the order of data points in the context dataset \mathcal{D} or the order at which we make predictions should not affect the probability of the data (i.e., the data is exchangeable). We also expect an *invariance* in the ordering of the input dimensions. While the posterior distribution need not possess symmetry in the input dimensions, the prior carries no information on the particular problem at hand, and so cannot favour one input over another. While a network can be encouraged to display invariances by manipulating the loss function during training or by data augmentations, it is preferable to instead enforce an invariance from the outset, by hard-wiring this behaviour into the architecture. The architecture used for the noise model is shown in fig. 3.

3.1 Dataset size and dimensionality agnosticity

As shown in fig. 3, the NDP’s noise model operates on batches of B datasets, where each dataset consists of N input and corresponding outputs. We assume that the inputs are D -dimensional (i.e., $\mathcal{X} = \mathbb{R}^D$) and that the outputs are one-dimensional.

A useful property of the NDP architecture is that it is agnostic to dataset size N and dimension D . That is, the weights of the network do *not* depend on N nor D , and the outputs will simply adapt to the shape of the corresponding inputs. To achieve this functionality, NDPs start with preprocessing the inputs ($x_t \in \mathbb{R}^{N \times D}$, $y_t \in \mathbb{R}^N$) to be of shape $[N, D, 2]$.¹ This shape allows the subsequent bi-dimensional attention blocks (explained next) to be N and D agnostic too. The preprocessing step consists of replicating the 1D outputs D times, to then group them with their corresponding inputs for each dimension. This gives D pairs $\{[x^d, y] \in \mathbb{R}^2\}_{d=1}^D$, as shown in the red box in fig. 3 and as listed in appendix E. The preprocessing step is followed by a fully-connected layer which projects the 2D inputs into an H -dimensional space. For the other input, time t , we follow Vaswani et al. [32] and use a cyclic 128-dimensional encoding (see appendix D.1 for details) followed by a dense layer to project it to the same H -dimensional space.

The dataset size and dimensionality agnosticity has important consequences: it is not required to train different NDPs for datasets with different size or dimensionality. This makes it possible to train a single model that handles downstream tasks with different N or D values, as illustrated in section 4.

¹In the coming sections we ignore the batch dimension B , as all operations simply parallelise over it.

3.2 Bi-dimensional Equivariant Attention Block

Our newly proposed bi-dimensional attention block is the workhorse of the NDP model. It acts on inputs $(\mathbf{x}_t, \mathbf{y}_t)$ and t after they are preprocessed and embedded into an H -dimensional space. At its core, the component consists of two multi-head self-attention (MHSA) layers [32]. The MHSA layers act on different axes of the input: one attends to the input dimension axis, while the other attends across the dataset sequence axis. The outputs of the two are subsequently summed and passed through a non-linearity. This process is repeated multiple times by feeding the output back into the next bi-dimensional attention block using residual connections, as illustrated in fig. 3.

We now show that this block is *equivariant* to the order of the dimensions and dataset sequence (i.e., shuffling the rows and/or columns of the input will shuffle the output in the same way). Therefore, let $\mathbf{A}_t : \mathbb{R}^{N \times D \times H} \rightarrow \mathbb{R}^{N \times D \times H}$, $\mathbf{s} \mapsto \mathbf{A}_t(\mathbf{s})$ be the bi-dimensional attention block. It acts on inputs \mathbf{s}_t which are created from $(\mathbf{x}_t, \mathbf{y}_t)$, as shown in the diagram. The following propositions hold:

Proposition 1. *Let Π_N be the set of all permutations of indices $\{1, \dots, N\}$. Let $\mathbf{s} \in \mathbb{R}^{N \times D \times H}$ and $(\pi_n \circ \mathbf{s}) \in \mathbb{R}^{N \times D \times H}$ denote a tensor where the ordering of indices in the first dimension (i.e., N) are given by $\pi_n \in \Pi_N$. Then, for all permutations $\pi_n \in \Pi_N$:*

$$\pi_n \circ \mathbf{A}_t(\mathbf{s}) = \mathbf{A}_t(\pi_n \circ \mathbf{s}).$$

Proposition 2. *Let Π_D be the set of all permutations of indices $\{1, \dots, D\}$. Let $\mathbf{s} \in \mathbb{R}^{N \times D \times H}$ and $(\pi_d \circ \mathbf{s}) \in \mathbb{R}^{N \times D \times H}$ denote a tensor where the ordering of indices in the second dimension (i.e., D) are given by $\pi_d \in \Pi_D$. Then, for all permutations $\pi_d \in \Pi_D$:*

$$\pi_d \circ \mathbf{A}_t(\mathbf{s}) = \mathbf{A}_t(\pi_d \circ \mathbf{s}).$$

Proof. We include proofs for propositions 1 and 2 in the supplementary (appendix C). \square

Given that the permutations π_n and π_d act on different axes of the tensor, we show in appendix C that they are compatible and commutative. This renders the bi-dimensional attention block \mathbf{A}_t simultaneously *equivariant* to both the dataset’s sequence, and its input dimensions.

3.3 Noise model outputs: invariant to dimension and equivariant to sequence order

NDP’s noise model outputs two key elements of the reverse process: $\epsilon_\theta^x(\cdot)$ predicts the noise added to the inputs, while $\epsilon_\theta^y(\cdot)$ predicts the noise added to the outputs. Both are formed by summing the output of multiple bi-dimensional attention layers, as shown by the purple summation in the architecture diagram. Since this summation is an element-wise operation, it does not break the equivariance properties detailed above. After this operation, the noise model bifurcates since we require different properties for $\epsilon_\theta^x(\cdot)$ and $\epsilon_\theta^y(\cdot)$. We expect ϵ_x to be equivariant in N and D , but for ϵ_θ^y we expect an *invariance* in D . That is, the output of the function ϵ_θ^y should not be affected by shuffling the features of the dataset. Following Zaheer et al. [35], we can accommodate for this invariance by summing over the input dimension axis (D), as shown by the green summation in fig. 3. Summarising, using the notation from proposition 1 & 2, we prove in appendix C, that the noise model adheres to

$$\begin{aligned} \pi_n \circ \pi_d \circ \epsilon_\theta^x(\mathbf{x}_t, \mathbf{y}_t, t) &= \epsilon_\theta^x(\pi_n \circ \pi_d \circ \mathbf{x}_t, \pi_n \circ \mathbf{y}_t, t), \text{ and} \\ \pi_n \circ \epsilon_\theta^y(\mathbf{x}_t, \mathbf{y}_t, t) &= \epsilon_\theta^y(\pi_n \circ \pi_d \circ \mathbf{x}_t, \pi_n \circ \mathbf{y}_t, t). \end{aligned}$$

4 Experimental Evaluation

In this section we conduct experiments to illustrate several important features of NDPs, including their ability to produce high-quality conditional samples, their capability to marginalise over kernel hyperparameters, and their input dimensionality invariance. We then consider NDPs’ application to both high-dimensional Bayesian optimisation (BO) and a novel global optimisation strategy using the NDP’s ability to model the joint $p(\mathbf{x}_0, \mathbf{y}_0)$. All experiments share the same model architecture illustrated in fig. 3 with 5 bi-dimensional attention blocks. All model configurations are given in appendix D.1. The code can be found in the supplementary.

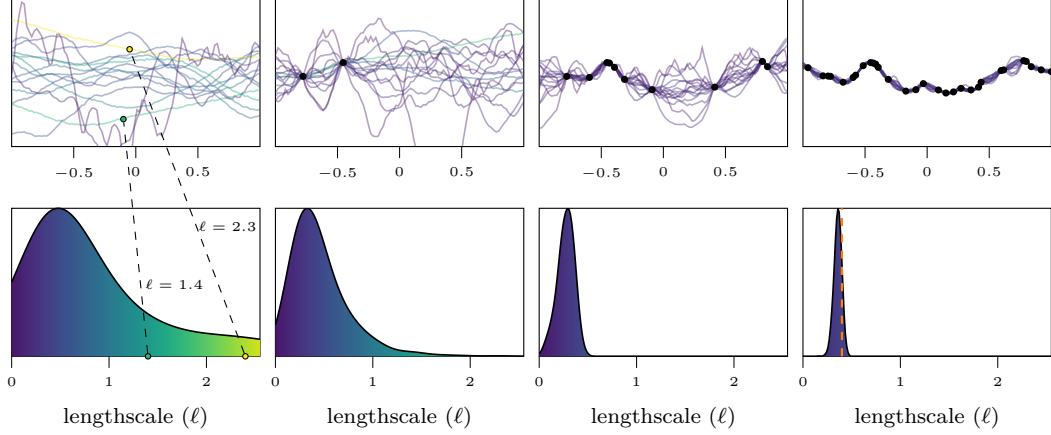


Figure 4: **Kernel lengthscale marginalisation:** Samples from the NDP, conditioned on an increasing number of data points (black dots), are illustrated in the top row. The colour of each sample corresponds to the lengthscale of a kernel that is most likely to produce the sample. The most likely lengthscale is derived from corresponding GPR model with the highest model evidence. The bottom row illustrates the distribution of lengthscales identified as most likely, across all samples. As more data points are provided, the distribution of likely lengthscales converges on the lengthscale that was used to produce the data (orange dashed line).

Datasets The training data for all experiments is created synthetically. We use GP prior samples, $\mathbf{y}_0 | \mathbf{x}_0 \sim \mathcal{N}(\mathbf{0}, k_\psi(\mathbf{x}_0, \mathbf{x}_0) + \sigma^2 \mathbf{I})$, with a small fixed likelihood variance. The GPs are all defined on the input domain $[-1, 1]^D$. We focus on stationary kernels, k_ψ . The lengthscales are either fixed or sampled from a log-normal distribution. Numerical details of the data generation process are given in appendix D.1.

Conditional sampling To show that NDPs learn accurate distributions over functions which can be used to draw coherent samples, we start with a simple 1D regression task. Figure 2 (and fig. D.1 in the supplementary) illustrate posterior samples drawn from a GP, Attentive Latent NP (ALNP) [10], and our NDP. The ALNP and NDP are trained on prior samples from a Squared Exponential (SE) kernel with a lengthscale of 0.2. For the ALNP we used a pretrained model from a reference implementation [3]. While the ALNP does not suffer from the underfitting known to occur in conventional NPs, the behaviour of the samples far from the datapoints is not an accurate reflection of their true functional form, given by the GP ground truth. The samples from the NDPs are seen to more closely resemble the target distribution.

Hyperparameter marginalisation Conventionally, GP models are trained by maximising the likelihood of the hyperparameters. Ideally, Bayesian inference is performed by marginalising the hyperparameters, which can lead to significant performance improvements, albeit at an extra computational cost [13, 26]. A key capability of the NDP is its ability to produce realistic conditional samples across the full gamut of data on which it was trained. It can therefore in effect marginalise over the different hyperparameters it was exposed to, or even different kernels. Figure 4 demonstrates how the model produces samples from a range of different lengthscales, and that it narrows down on the true lengthscale as more data is observed. This model was trained on samples from a GP with a Matérn- $\frac{3}{2}$ kernel, with a variety of lengthscales sampled from $\log \mathcal{N}(\log(0.5), \sqrt{0.5})$.

Dimensionality invariance on two-dimensional data NDP’s dimensionality invariance means that it assumes no explicit ordering in the columns of a dataset. This is a common property of many tabular datasets (e.g., UCI repository [29]), yet it is heavily under-exploited in the literature [15]. To illustrate that this property is encoded into a NDP, we train it on samples originating from a GP with a SE kernel containing lengthscales $\ell = [0.2, 0.8]$ (i.e., one short, one long). From fig. 5 (a) and (b) we observe that the model generates samples corresponding to both $\ell = [0.2, 0.8]$ and $\ell = [0.8, 0.2]$, reflecting the model’s invariance to the input order. Further, in (c) and (d), we plot posterior samples and see that the predictions match the observed values closely. In (e) we compare

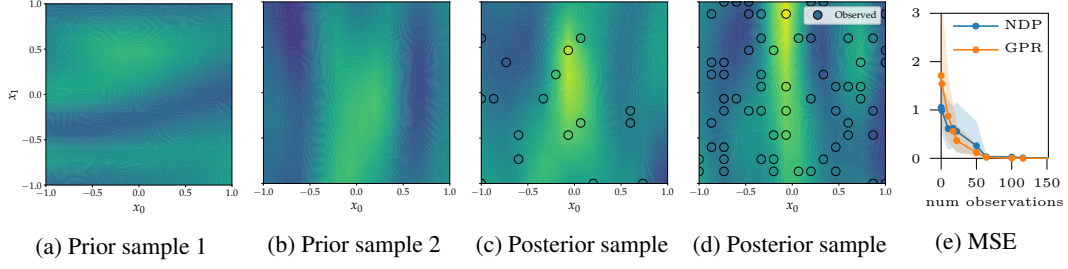


Figure 5: **2D regression:** Samples from the prior and posterior demonstrate the model’s dimensional invariance. Posterior samples are conditioned on observations (circles), where the colour of the circle corresponds to the ground truth value the model is conditioning on.

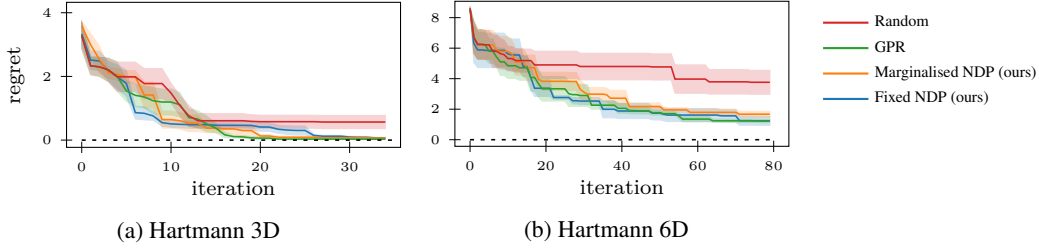


Figure 6: **Bayesian Optimisation:** The regret of different probabilistic models used in Thompson sampling based Bayesian Optimisation on a 3D (*left*) and a 6D (*right*) problem. The uncertainty estimates are based on repeating the experiment five times with different random seeds.

the NDP’s predictive performance measured in mean squared error (MSE) on a held-out dataset with a GPR model. Both MSEs tend to zero as more data is observed.

Higher-dimensional BO In this experiment we highlight that NDPs can be used in problems with $D \geq 3$. We tackle 3D and 6D minimisation problems, given in appendix D.3, using discrete Thompson sampling BO [24, 5, 30]. In this setting, the probabilistic model is used as surrogate of an expensive black-box objective. At each iteration the surrogate is evaluated at 128 random locations in the input domain and the input corresponding to the minimum value is selected as the next query point. The objective is evaluated at this location and added to the context dataset. Figure 6 shows the regret (distance from the true minimum) for different models. We observe that the NDP almost matches the performance of GPR, which is the gold standard model on this type of task. The important difference between GPR and the NDP is that the NDP requires *no training* during the BO loop, whereas GPR is retrained at every step.

Optimisation using density estimation Instead of obtaining samples from $p(\mathbf{y}^* | \mathbf{x}^*, \mathcal{D})$, we could conceive of a different optimisation strategy by taking advantage of the NDP’s ability to model the full joint distribution $p(\mathbf{x}^*, \mathbf{y}^* | \mathcal{D})$. Consider conditioning the NDP model on our current belief about the minimum value \mathbf{y}^* . This allows us to obtain samples from $p(\mathbf{x}^* | \mathbf{y}^*)$ which contain information about where the minima lies in the input domain according to the model. In fig. 7 we illustrate a global optimisation routine using this idea. In each step, we sample a target from $p(\mathbf{y}^*)$, which describes our belief about the minima. For the figure, we used a truncated Normal for $p(\mathbf{y}^*)$, where the range is specified using the already observed data (we refer to appendix D.4 for further details). The next query point is selected by sampling $p(\mathbf{x}^* | \mathbf{y}^*, \mathcal{D})$, thereby systematically seeking out the global minimum. This experiment showcases NDP’s ability to model the complex interaction between inputs and outputs of function—a task on which it was not explicitly trained.

5 Related work

We briefly discussed related work in the introduction. Here, we dive a bit deeper in related methods that focus on using neural networks to describe a probability distribution over functions.

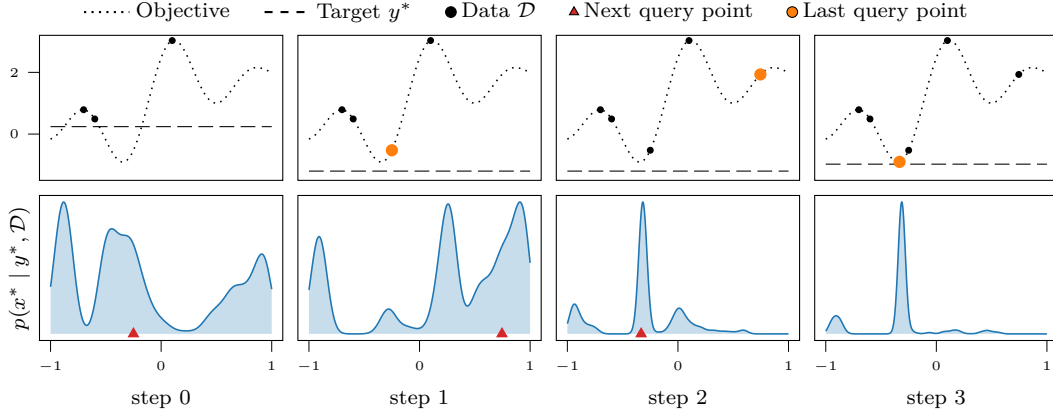


Figure 7: **Global optimisation** by diffusing the input locations. We condition the model at each step on a target y^* value (dashed line), and use the NDP to sample from $p(y^* | x^*, \mathcal{D})$, i.e. the posterior distribution of the input location which satisfies this new objective value. The panels in the upper row illustrate the progression of the optimisation. In the lower row, the blue distribution corresponds to the model’s belief about where the target lies, while the red triangles mark the selected query point.

Neural processes family Neural processes [7, 8] are a family of models which are closely related to NDPs, in that they utilise deep neural networks to define a rich probability distribution over functions. A NP consists of two components: an encoder and a decoder. The encoder is used to embed a context dataset into a latent representation, which is then used by the decoder to make predictions at target points. *Conditional NPs* [7] predict only the marginals of the posterior, which makes it impossible to draw coherent samples from the model. *Latent NPs* [8] try to alleviate this problem by incorporating latent variables, but this introduces difficulties stemming from approximate inference.

Although NPs have similar properties to NDPs, they do not incorporate dimensional invariance and they typically suffer from underfitting to the context set, leading to overestimated uncertainties, and samples which do not pass through the context points. Several improvements to this approach have been proposed, including attention-based NPs [10] and Gaussian NPs [2, 18]; however to the best of our knowledge none have been demonstrated to perform inference in $D > 3$.

Neural networks for speeding up GP training and model selection There has been a growing body of work demonstrating how deep neural network architectures offer a promising approach to amortising the computationally intensive calculations associated with GPs. For example, Liu et al. [14] used a transformer to predict the hyperparameters of a spectral mixture kernel, while Simpson et al. [25] used a transformer to recommend a suitable GP kernel for a given dataset.

6 Conclusion

We proposed Neural Diffusion Processes (NDPs), a denoising diffusion model approach for learning probabilities on function spaces, and generating prior and conditional samples of functions. NDPs generalise diffusion models to infinite-dimensional function spaces by allowing the indexing of random variables. We introduced a new neural network building component, namely the bi-dimensional attention block, which wires dimension and sequence equivariance into the neural network architecture such that it behaves like a stochastic process. We empirically show that this model is able to capture functional distributions that are close to the true Bayesian posterior.

Limitations and Future Work As with other diffusion models, we found that the sample quality from a NDP improves with the number of diffusion steps T . This does however lead to slower inference times relative to other architectures such as GANs. Techniques for accelerating the inference process could be incorporated to ameliorate this issue. The method proposed by Watson et al. [33] is of particular interest for NDPs as we have a principled and differentiable metric to assess sample quality, namely the corresponding GP’s marginal likelihood. Finally, parameterising the samples in the Fourier domain, using e.g. [21, 4], could be an interesting alternative approach.

References

- [1] J. Berkeley, H. B. Moss, A. Artemev, S. Pascual-Diaz, U. Granta, H. Stojic, I. Couckuyt, J. Qing, N. Loka, A. Paleyes, S. W. Ober, and V. Picheny. Trieste, 2022. URL: <https://github.com/secondmind-labs/trieste>. Cited on page 20.
- [2] W. P. Bruinsma, J. Requeima, A. Y. Foong, J. Gordon, and R. E. Turner. The Gaussian neural process. In *Advances in Approximate Bayesian Inference*, 2021. Cited on pages 1, 9.
- [3] Y. Dubois, J. Gordon, and A. Y. Foong. Neural process family. <http://yanndubs.github.io/Neural-Process-Family/>. Cited on pages 7, 19.
- [4] V. Dutordoir, N. Durrande, and J. Hensman. Sparse Gaussian processes with spherical harmonic features. In *International Conference on Machine Learning*, 2020. Cited on page 9.
- [5] V. Dutordoir, N. Knudde, J. van der Hertten, I. Couckuyt, and T. Dhaene. Deep Gaussian Process metamodeling of sequentially sampled non-stationary response surfaces. In *Winter Simulation Conference*, 2017. Cited on page 8.
- [6] V. Fortuin, D. Baranchuk, G. Rätsch, and S. Mandt. GP-VAE: Deep probabilistic time series imputation. In *International Conference on Artificial Intelligence and Statistics*, 2020. Cited on page 1.
- [7] M. Garnelo, D. Rosenbaum, C. Maddison, T. Ramalho, D. Saxton, M. Shanahan, Y. W. Teh, D. J. Rezende, and S. M. A. Eslami. Conditional Neural Processes. In *International Conference on Machine Learning*, 2018. Cited on pages 4, 9.
- [8] M. Garnelo, J. Schwarz, D. Rosenbaum, F. Viola, D. J. Rezende, S. M. A. Eslami, and Y. W. Teh. Neural processes. *arXiv preprint arXiv:1807.01622*, 2018. Cited on pages 1, 4, 9.
- [9] J. Ho, A. Jain, and P. Abbeel. Denoising diffusion probabilistic models. In *Neural Information Processing Systems*, 2020. Cited on pages 1–3, 12.
- [10] H. Kim, A. Mnih, J. Schwarz, M. Garnelo, S. M. A. Eslami, D. Rosenbaum, O. Vinyals, and Y. W. Teh. Attentive neural processes. In *International Conference on Learning Representations*, 2019. Cited on pages 4, 7, 9.
- [11] D. P. Kingma, T. Salimans, B. Poole, and J. Ho. Variational diffusion models. In *Neural Information Processing Systems*, 2021. Cited on page 3.
- [12] Z. Kong, W. Ping, J. Huang, K. Zhao, and B. Catanzaro. Diffwave: A versatile diffusion model for audio synthesis. In *International Conference on Learning Representations*, 2020. Cited on page 1.
- [13] V. Lalchand and C. E. Rasmussen. Approximate inference for fully Bayesian Gaussian process regression. In *Advances in Approximate Bayesian Inference*, 2020. Cited on pages 1, 7.
- [14] S. Liu, X. Sun, P. J. Ramadge, and R. P. Adams. Task-agnostic amortized inference of Gaussian process hyperparameters. In *Neural Information Processing Systems*, 2020. Cited on page 9.
- [15] J. R. Lloyd, P. Orbanz, Z. Ghahramani, and D. M. Roy. Random function priors for exchangeable arrays with applications to graphs and relational data. In *Neural Information Processing Systems*, 2012. Cited on page 7.
- [16] A. Lugmayr, M. Danelljan, A. Romero, F. Yu, R. Timofte, and L. Van Gool. RePaint: Inpainting using denoising diffusion probabilistic models. *arXiv preprint arXiv:2201.09865*, 2022. Cited on pages 4, 14.
- [17] S. Luo and W. Hu. Diffusion probabilistic models for 3d point cloud generation. In *Computer Vision and Pattern Recognition*, 2021. Cited on page 1.
- [18] S. Markou, J. Requeima, W. Bruinsma, and R. Turner. Efficient Gaussian Neural Processes for Regression. *arXiv preprint arXiv:2108.09676*, 2021. Cited on pages 1, 9.
- [19] S. Mishra, S. Flaxman, T. Berah, M. Pakkanen, H. Zhu, and S. Bhatt. piVAE: Encoding stochastic process priors with variational autoencoders. *arXiv preprint arXiv:2002.06873*, 2020. Cited on page 1.
- [20] A. Nichol, P. Dhariwal, A. Ramesh, P. Shyam, P. Mishkin, B. McGrew, I. Sutskever, and M. Chen. Glide: Towards photorealistic image generation and editing with text-guided diffusion models. *arXiv preprint arXiv:2112.10741*, 2021. Cited on pages 1, 18.
- [21] A. Rahimi and B. Recht. Random features for large-scale kernel machines. In *Neural Information Processing Systems*, 2007. Cited on page 9.
- [22] A. Ramesh, P. Dhariwal, A. Nichol, C. Chu, and M. Chen. Hierarchical text-conditional image generation with CLIP latents. *arXiv preprint arXiv:2204.06125*, 2022. Cited on page 1.

- [23] C. E. Rasmussen and C. K. Williams. *Gaussian processes for machine learning*. MIT Press, 2006. Cited on page 1.
- [24] B. Shahriari, K. Swersky, Z. Wang, R. P. Adams, and N. De Freitas. Taking the human out of the loop: A review of Bayesian optimization. *Proceedings of the IEEE*, 2015. Cited on page 8.
- [25] F. Simpson, I. Davies, V. Lalchand, A. Vullo, N. Durrande, and C. E. Rasmussen. Kernel identification through transformers. In *Neural Information Processing Systems*, 2021. Cited on page 9.
- [26] F. Simpson, V. Lalchand, and C. E. Rasmussen. Marginalised Gaussian processes with nested sampling. In *Neural Information Processing Systems*, 2021. Cited on page 7.
- [27] J. Sohl-Dickstein, E. A. Weiss, N. Maheswaranathan, and S. Ganguli. Deep unsupervised learning using nonequilibrium thermodynamics. *arXiv preprint arXiv:1503.03585*, 2015. Cited on pages 1, 2, 12.
- [28] Y. Song and S. Ermon. Improved techniques for training score-based generative models. In *Neural Information Processing Systems*, volume 33, 2020. Cited on pages 1, 2.
- [29] UCI Machine Learning Repository. <https://archive.ics.uci.edu/ml/index.php>. Cited on page 7.
- [30] S. Vakili, H. Moss, A. Artemev, V. Dutordoir, and V. Picheny. Scalable Thompson Sampling using Sparse Gaussian Process Models. In *Neural Information Processing Systems*, 2021. Cited on page 8.
- [31] M. van der Wilk, V. Dutordoir, S. John, A. Artemev, V. Adam, and J. Hensman. A framework for interdomain and multioutput Gaussian processes. *arxiv preprint arXiv:2003.01115*, 2020. Cited on page 19.
- [32] A. Vaswani, N. Shazeer, N. Parmar, J. Uszkoreit, L. Jones, A. N. Gomez, Ł. Kaiser, and I. Polosukhin. Attention is all you need. In *Neural Information Processing Systems*, 2017. Cited on pages 5, 6, 16–19.
- [33] D. Watson, W. Chan, J. Ho, and M. Norouzi. Learning fast samplers for diffusion models by differentiating through sample quality. In *International Conference on Learning Representations*, 2021. Cited on page 9.
- [34] M. Xu, L. Yu, Y. Song, C. Shi, S. Ermon, and J. Tang. Geodiff: A geometric diffusion model for molecular conformation generation. *arXiv preprint arXiv:2203.02923*, 2022. Cited on page 1.
- [35] M. Zaheer, S. Kottur, S. Ravanbakhsh, B. Poczos, R. R. Salakhutdinov, and A. J. Smola. Deep Sets. In *Neural Information Processing Systems*, 2017. Cited on pages 6, 18.

Neural Diffusion Processes: Supplementary

A Derivation of the Loss

In this section we derive the objective given in eq. (5), following a path similar to that presented in Ho et al. [9]. Let $\mathbf{s}_t = (\mathbf{x}_t, \mathbf{y}_t)$ be the state that combines both the inputs and observations. We wish to find the set of parameters θ which maximise the likelihood given the initial state, $p_\theta(\mathbf{s}_0)$. While a direct evaluation of the likelihood appears intractable,

$$p_\theta(\mathbf{s}_0) = \int p_\theta(\mathbf{s}_{0:T}) d\mathbf{s}_{1:T},$$

this may be recast in a form which allows for a comparison to be drawn between the forward and reverse trajectories [27]

$$p_\theta(\mathbf{s}_0) = \int p_\theta(\mathbf{s}_T) q(\mathbf{s}_{1:T} | \mathbf{s}_0) \prod_{t=1}^T \frac{p_\theta(\mathbf{s}_{t-1} | t)}{q(\mathbf{s}_t | \mathbf{s}_{t-1})} d\mathbf{s}_{1:T}.$$

The appeal of introducing the reverse process is that it is tractable when conditioned on the first state \mathbf{s}_0 , taking a Gaussian form

$$q(\mathbf{s}_{t-1} | \mathbf{s}_t, \mathbf{s}_0) = \mathcal{N}(\mathbf{s}_{t-1} | \tilde{\boldsymbol{\mu}}(\mathbf{s}_t, \mathbf{s}_0), \tilde{\beta}_t \mathbf{I}).$$

Our loss function reflects a lower bound on the negative log likelihood

$$\mathbb{E}[-\log p_\theta(\mathbf{s}_0)] \leq \mathbb{E}_{q(\mathbf{s}_{0:T})} \left[\log \frac{q(\mathbf{s}_{1:T} | \mathbf{s}_0)}{p_\theta(\mathbf{s}_{0:T})} \right] := \mathcal{L}_\theta,$$

which may be decomposed into two edge terms and a sum over the intermediate steps, as follows

$$\mathcal{L}_\theta = \mathbb{E}_q \left[L_T + \sum_{t=2}^T L_{t-1} + L_0 \right],$$

where

$$\begin{aligned} L_0 &= -\log p_\theta(\mathbf{s}_0 | \mathbf{s}_1), \\ L_{t-1} &= \text{KL}(q(\mathbf{s}_{t-1} | \mathbf{s}_t, \mathbf{s}_0) \| p_\theta(\mathbf{s}_{t-1} | \mathbf{s}_t)), \\ L_T &= \text{KL}(q(\mathbf{s}_T | \mathbf{s}_0) \| p_\theta(\mathbf{s}_T)). \end{aligned} \tag{8}$$

We can write

$$L_{t-1} = \mathbb{E}_{\mathbf{s}_0, \epsilon} \left[\frac{1}{2\sigma^2} \|\tilde{\boldsymbol{\mu}}(\mathbf{s}_t, \mathbf{s}_0) - \boldsymbol{\mu}_\theta(\mathbf{s}_t, t)\|^2 \right], \tag{9}$$

where the mean is a function of the previous and first state

$$\tilde{\boldsymbol{\mu}}(\mathbf{s}_t, \mathbf{s}_0) = \frac{\sqrt{\alpha_t}(1 - \bar{\alpha}_{t-1})}{1 - \bar{\alpha}_t} \mathbf{s}_t + \frac{\sqrt{\bar{\alpha}_{t-1}}\beta_t}{1 - \bar{\alpha}_t} \mathbf{s}_0$$

and the variance

$$\tilde{\beta}_t = \frac{1 - \bar{\alpha}_{t-1}}{1 - \bar{\alpha}_t} \beta_t.$$

It is helpful to consider the relationship between the initial and final states

$$\mathbf{s}_0 = \frac{1}{\sqrt{\bar{\alpha}_t}} (\mathbf{s}_t - \sqrt{1 - \bar{\alpha}_t} \boldsymbol{\epsilon}_s),$$

where $\varepsilon_s = (\varepsilon_x, \varepsilon_y)$, so that we can rewrite the mean as

$$\tilde{\mu}(s_t, \varepsilon_s) = \frac{1}{\sqrt{\alpha_t}}(s_t - \frac{\beta_t}{\sqrt{1 - \alpha_t}}\varepsilon_s). \quad (10)$$

Equation 9 can now be expressed as

$$L_{t-1} = \mathbb{E}_{s_0, \varepsilon_s} \left[\frac{\beta_t^2}{2\sigma^2\alpha_t(1 - \bar{\alpha}_t)} \|\varepsilon_s - \epsilon_\theta^s\|^2 \right]. \quad (11)$$

Finally, since the variance schedule is fixed, and the edge terms are not found to improve empirical performance, our simplified training objective is given by

$$\mathcal{L}_\theta = \mathbb{E}_{x_0, y_0, \varepsilon_x, \varepsilon_y, t} \left[\|\varepsilon_x - \epsilon_\theta^x(x_t, y_t, t)\|^2 + \|\varepsilon_y - \epsilon_\theta^y(x_t, y_t, t)\|^2 \right]. \quad (12)$$

B Algorithms

In this section we list pseudo-code for training and sampling NDPs. The code to handle the special case of deterministic input locations (section 2.2) is marked by ‘OR’. In this case, there are no intermediate states for the inputs x_t , and the input to the noise model for y is simply x_0 .

B.1 Training

The training procedure is concerned with fitting the parameters of the NDP’s noise model neural network, with outputs $\epsilon_\theta^x, \epsilon_\theta^y$, such that they can accurately predict the noise that was added to the corrupted function draws. In each iteration, we create a batch of datasets, each originating from a Gaussian process draw. We stress that the number of datapoints and even the input dimensionality of the datasets can vary within the training procedure.

Algorithm 1 Training

input Input distribution $q(x_0)$ and covariance function k_ψ , with prior over hyperparameters p_ψ . Noise schedule β_t for $t \in \{1, 2, \dots, T\}$. A loss function L (e.g., MSE or MAE).

begin

Precompute $\gamma_t = \sqrt{1 - \bar{\alpha}_t}$ and $\bar{\alpha}_t = \prod_{j=1}^t (1 - \beta_j)$.

for $i = 1, 2, \dots, N_{\text{iter}}$ **do**

Sample $x_0 \sim q(x_0)$, $\psi \sim p_\psi$, $y_0 \sim \mathcal{N}(\mathbf{0}, k_\psi(x_0, x_0) + \sigma^2 \mathbf{I})$.

Sample $\varepsilon_x, \varepsilon_y \sim \mathcal{N}(\mathbf{0}, \mathbf{I})$, and $t \sim \mathcal{U}(\{1, \dots, T\})$.

Compute $x_t = \sqrt{\bar{\alpha}_t}x_0 + \gamma_t\varepsilon_x$ and $y_t = \sqrt{\bar{\alpha}_t}y_0 + \gamma_t\varepsilon_y$.

eq. (3)

Update θ using gradient $\nabla_\theta [L(\varepsilon_x, \epsilon_\theta^x(x_t, y_t, t)) + L(\varepsilon_y, \epsilon_\theta^y(x_t, y_t, t))]$.

eq. (5)

OR, in the case that we only diffuse on the observations:

eq. (7)

Update θ using gradient $\nabla_\theta L(\varepsilon_y, \epsilon_\theta^y(x_0, y_t, t))$.

B.2 Prior and Conditional Sampling

In practice, the code to sample the prior is a special case of the conditional code with an empty context dataset. However, here we list them both for the clarity of the exposition.

Algorithm 2 Prior Sampling

input A pretrained NDP noise model $\epsilon_\theta^x(\cdot)$ and $\epsilon_\theta^y(\cdot)$. Precomputed γ_t and $\bar{\alpha}_t$ from a given noise schedule β_t .

begin

Sample a random initial state \mathbf{x}_T and \mathbf{y}_T from $\mathcal{N}(\mathbf{0}, \mathbf{I})$.

for $t = T, T-1, \dots, 1$ **do**

Sample using backward kernel:

eq. (4)

$$\begin{bmatrix} \mathbf{x}_{t-1} \\ \mathbf{y}_{t-1} \end{bmatrix} \sim \mathcal{N}\left(\frac{1}{\sqrt{1-\beta_t}}\left(\begin{bmatrix} \mathbf{x}_t \\ \mathbf{y}_t \end{bmatrix} - \frac{\beta_t}{\gamma_t} \begin{bmatrix} \epsilon_\theta^x(\mathbf{x}_t, \mathbf{y}_t, t) \\ \epsilon_\theta^y(\mathbf{x}_t, \mathbf{y}_t, t) \end{bmatrix}\right), \frac{\gamma_t^2}{\gamma_{t-1}^2} \beta_t \mathbf{I}\right).$$

OR, in the case that we only diffuse on the observations and the inputs \mathbf{x}_0 are given:

$$\mathbf{y}_{t-1} \sim \mathcal{N}\left(\frac{1}{\sqrt{1-\beta_t}}\left(\mathbf{y}_t - \frac{\beta_t}{\gamma_t} \epsilon_\theta^y(\mathbf{x}_0, \mathbf{y}_t, t)\right), \frac{\gamma_t^2}{\gamma_{t-1}^2} \beta_t \mathbf{I}\right).$$

return $(\mathbf{x}_0, \mathbf{y}_0)$

The conditional sampling algorithm is based on recent advances in image inpainting using diffusion models [16]. In algorithm 3, for optimal results, we follow Lugmayr et al. [16] and use a re-sampling step which mixes the predictions with the context dataset. In all our experiments U was set to 5.

Algorithm 3 Conditional Sampling

input A context dataset $\mathcal{D} = \{([\mathbf{x}_0^c]_i \in \mathcal{X}, [\mathbf{y}_0^c]_i \in \mathbb{R})\}_{i=1}^N$. A pretrained NDP noise model $\epsilon_\theta^x(\cdot)$ and $\epsilon_\theta^y(\cdot)$. Precomputed γ_t and $\bar{\alpha}_t$ from a given noise schedule β_t .

begin

Let the augmented states be $\mathbf{x}_T \in \mathcal{X}^{N+1}$ and $\mathbf{y}_T \in \mathbb{R}^{N+1}$. Sample them according to $\mathbf{x}_T \sim \mathcal{N}(\mathbf{0}, \mathbf{I})$ and $\mathbf{y}_T \sim \mathcal{N}(\mathbf{0}, \mathbf{I})$.

Create a mask $m = [0, \dots, 0, 1] \in \mathbb{R}^{N+1}$ indicating the positions of the unknown state.

for $t = T, T-1, \dots, 1$ **do**

for $u = 1, \dots, U$ **do**

Sample backward from augmented intermediate state:

eq. (4)

$$\begin{bmatrix} \mathbf{x}_{t-1} \\ \mathbf{y}_{t-1} \end{bmatrix} \sim \mathcal{N}\left(\frac{1}{\sqrt{1-\beta_t}}\left(\begin{bmatrix} \mathbf{x}_t \\ \mathbf{y}_t \end{bmatrix} - \frac{\beta_t}{\gamma_t} \begin{bmatrix} \epsilon_\theta^x(\mathbf{x}_t, \mathbf{y}_t, t) \\ \epsilon_\theta^y(\mathbf{x}_t, \mathbf{y}_t, t) \end{bmatrix}\right), \frac{\gamma_t^2}{\gamma_{t-1}^2} \beta_t \mathbf{I}\right).$$

Select unknown part from the augmented state using the mask:

$$\mathbf{x}_{t-1} = m \odot \mathbf{x}_{t-1} \quad \text{and} \quad \mathbf{y}_{t-1} = m \odot \mathbf{y}_{t-1}$$

Sample context points $(t-1)$ -steps forward from context dataset

eq. (3)

$$\begin{bmatrix} \mathbf{x}_{t-1}^c \\ \mathbf{y}_{t-1}^c \end{bmatrix} \sim \mathcal{N}\left(\begin{bmatrix} \mathbf{x}_{t-1}^c \\ \mathbf{y}_{t-1}^c \end{bmatrix} \mid \sqrt{\bar{\alpha}_{t-1}} \begin{bmatrix} \mathbf{x}_0^c \\ \mathbf{y}_0^c \end{bmatrix}, \gamma_{t-1}^2 \mathbf{I}_n\right)$$

Create new augmented intermediate state using the forward sampled context dataset and the unknown intermediate state:

$$\mathbf{x}_{t-1} = \begin{bmatrix} \mathbf{x}_{t-1}^c \\ \mathbf{x}_{t-1} \end{bmatrix} \quad \text{and} \quad \mathbf{y}_{t-1} = \begin{bmatrix} \mathbf{y}_{t-1}^c \\ \mathbf{y}_{t-1} \end{bmatrix}.$$

Diffuse by one step

eq. (2)

$$\begin{bmatrix} \mathbf{x}_t \\ \mathbf{y}_t \end{bmatrix} \sim \mathcal{N}\left(\begin{bmatrix} \mathbf{x}_t \\ \mathbf{y}_t \end{bmatrix} \mid \sqrt{1-\beta_t} \begin{bmatrix} \mathbf{x}_{t-1} \\ \mathbf{y}_{t-1} \end{bmatrix}, \beta_t \mathbf{I}\right)$$

return $(\mathbf{x}_0, \mathbf{y}_0)$

C Proofs

In this section, we shall formally demonstrate that NDP’s noise model adheres to the symmetries associated with permutations of the datapoint orderings and the permutations of the input dimensions. We do this by first proving equivariance of its main building block: the bi-dimensional attention block. From this, we can then straightforwardly prove the equivariance and invariance properties that hold for the NDP’s noise model. Before that, we start by setting the notation.

C.1 Notation, Definitions and Preliminary lemmas

Notation. Let $\mathbf{s} \in \mathbb{R}^{N \times D \times H}$ be a tensor of rank (or dimension) three, where we refer to each dimension according to the following convention:

$$\text{shape}(\mathbf{s}) = [N, D, H].$$

dim. 1: sequence length
 dim. 3: embedding
 dim. 2: input dimensionality

In the next definitions we will use NumPy-based indexing and slicing notation. We assume the reader is familiar with this convention. Most notably, we use a colon (:) to reference every element in a dimension.

Definition 1. Let Π_N be the set of all permutations of indices $\{1, \dots, N\}$. Let $\pi_n \in \Pi_N$ and $\mathbf{s} \in \mathbb{R}^{N \times D \times H}$. Then $(\pi_n \circ \mathbf{s}) \in \mathbb{R}^{N \times D \times H}$ denotes a tensor where the ordering of indices in the first dimension are reshuffled (i.e., permuted) according to π_n . We write

$$\pi_n \circ \mathbf{s} = \mathbf{s}_{\pi_n(1), \pi_n(2), \dots, \pi_n(N); :, :}$$

Definition 2. Let Π_D be the set of all permutations of indices $\{1, \dots, D\}$. Let $\pi_d \in \Pi_D$ and $\mathbf{s} \in \mathbb{R}^{N \times D \times H}$. Then $(\pi_d \circ \mathbf{s}) \in \mathbb{R}^{N \times D \times H}$ denotes a tensor where the ordering of indices in the second dimension are reshuffled (i.e., permuted) according to π_d . We write

$$\pi_d \circ \mathbf{s} = \mathbf{s}_{:, \pi_d(1), \pi_d(2), \dots, \pi_d(D); :}$$

Definition 3. A function $f : \mathbb{R}^{N \times D \times H} \rightarrow \mathbb{R}^{N \times D \times H}$ is equivariant to Π if for any permutation $\pi \in \Pi$, we have

$$f(\pi \circ \mathbf{s}) = \pi \circ f(\mathbf{s}).$$

Equivariance in layman’s terms means that the output of a function is affected “in the same way” as the input. In our case, Π will be Π_N and/or Π_D .

Definition 4. A function $f : \mathbb{R}^{N \times D \times H} \rightarrow \mathbb{R}^{N \times D \times H}$ is invariant to Π if for any permutation $\pi \in \Pi$, we have

$$f(\pi \circ \mathbf{s}) = f(\mathbf{s}).$$

Invariance in layman’s terms means that the output is not affected by a permutation of the inputs.

Lemma 1. The composition of equivariant functions is equivariant.

Proof. Let f and g be equivariant to Π , then for all $\pi \in \Pi$:

$$(f \circ g)(\pi \circ \mathbf{s}) = f(g(\pi \circ \mathbf{s})) = f(\pi \circ g(\mathbf{s})) = \pi \circ f(g(\mathbf{s})),$$

which shows that the composition, $f \circ g$, is equivariant as well. \square

Lemma 2. An element-wise operation between equivariant functions remains equivariant.

Proof. Let f and g be equivariant to Π , then for all $\pi \in \Pi$ and an element-wise operation \oplus (e.g., addition), we have

$$(f \oplus g)(\pi \circ \mathbf{s}) = f(\pi \circ \mathbf{s}) \oplus g(\pi \circ \mathbf{s}) = (\pi \circ f(\mathbf{s})) \oplus (\pi \circ g(\mathbf{s})) = \pi \circ (f \oplus g).$$

which shows that the composition, $f \oplus g$, is equivariant as well. \square

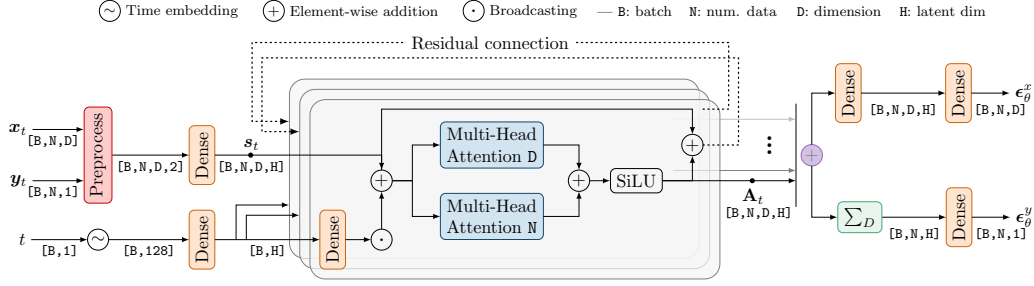


Figure C.1: Architecture of the **noise prediction model**, utilised at each step within the Neural Diffusion Process. The greyed box represents the **bi-dimensional** attention block, as discussed in Section 3.2.

Lemma 3. A function $f : \mathbb{R}^{N \times D \times H} \rightarrow \mathbb{R}^{N \times D \times H}$ which applies the same function g to all its rows, i.e. $f : s \mapsto [g(s_{1,:}), g(s_{2,:}), \dots, g(s_{N,:})]$ with $g : \mathbb{R}^{D \times H} \rightarrow \mathbb{R}^{D \times H}$ is equivariant in the first dimension.

Proof. Follows immediately from the structure of f . \square

C.2 Bi-dimensional Attention Block

With the notation, definitions and lemmas in place, we now prove that the bi-dimensional attention block is equivariant in its first and second dimension, respectively to permutations in the set Π_N and Π_D . We start this section by formally defining the bi-dimensional attention block and its main components attention components Attn_N and Attn_D . Finally, in appendix C.3 we prove the properties of the noise models ϵ_θ^x and ϵ_θ^y making use of the results in this section.

Definition 5. Ignoring the batch dimension B , let $\mathbf{A}_t : \mathbb{R}^{N \times D \times H} \rightarrow \mathbb{R}^{N \times D \times H}$; $s \mapsto \mathbf{A}_t(s)$ be the bi-dimensional attention block. As illustrated in fig. C.1, it operates on three dimensional tensors in $\mathbb{R}^{N \times D \times H}$ and applies attention across the first and second dimension using Attn_N and Attn_D , respectively. The final output $\mathbf{A}_t(s)$ is obtained by summing the two attention outputs, before applying an element-wise non-linearity.

We now proceed by defining the component Attn_D and its properties. Subsequently, in definition 7 we define Attn_N and its properties. Finally, we combine both to prove propositions 1 and 2 in the main paper about the bi-dimensional attention block.

Definition 6. Let $\text{Attn}_D : \mathbb{R}^{N \times D \times H} \rightarrow \mathbb{R}^{N \times D \times H}$ be a self-attention block [32] acting across D . Let σ be a softmax activation function operating on the last dimension of a tensor. Then, Attn_D is defined as

$$\text{Attn}_D(s)[n, d, h] = \sum_{d'=1}^D \Sigma_{n,d,d'}(s) s_{n,d',h}^v, \quad \text{where} \quad \Sigma_{n,d,d'}(s) = \sigma\left(\frac{1}{\sqrt{H}} \sum_l s_{n,d,\ell}^k s_{n,d',\ell}^q\right)$$

given a linear projection of the inputs s which maps them into keys (k), queries (q) and values (v)

$$s_{n,d,\ell}^k = \sum_j s_{n,d,j} \mathbf{W}_{j,\ell}^k, \quad s_{n,d',\ell}^q = \sum_j s_{n,d,j} \mathbf{W}_{j,\ell}^q, \quad s_{n,d',h}^v = \sum_j s_{n,d,j} \mathbf{W}_{j,h}^v.$$

Proposition 3. Attn_D is equivariant to Π_N and Π_D (i.e., across sequence length and input dimensionality).

Proof. We prove the equivariance to Π_N and Π_D separately. First, from the definition we can see that Attn_D is a function that acts on each element row of s separately. Thus, by lemma 3, Attn_D is equivariant to Π_N .

Next, we want to prove equivariance to Π_D . We want to show that for all $\pi_d \in \Pi_D$:

$$\text{Attn}_D(\pi_d \circ s) = \pi_d \circ \text{Attn}_D(s).$$

The self-attention mechanism consists of a matrix multiplication of the attention matrix Σ and the projected inputs. We start by showing that the attention matrix is equivariant to permutations in Π_D

$$\begin{aligned}\Sigma_{n,d,d'}(\pi_d \circ \mathbf{s}) &= \sigma\left(\frac{1}{\sqrt{H}} \sum_{\ell} (\pi_d \circ \mathbf{s})_{n,d,\ell}^k (\pi_d \circ \mathbf{s})_{n,d,\ell}^q\right) \\ &= \sigma\left(\frac{1}{\sqrt{H}} \sum_{\ell,j} (\mathbf{s}_{n,\pi_d(d),j} \mathbf{W}_{j,\ell}^k) (\mathbf{s}_{n,\pi_d(d'),j} \mathbf{W}_{j,\ell}^q)\right) \\ &= \Sigma_{n,\pi_d(d),\pi_d(d')}(\mathbf{s})\end{aligned}$$

It remains to show that the final matrix multiplication step restores the row-equivariance

$$\begin{aligned}\text{Attn}_D(\pi_d \circ \mathbf{s}) &= \sum_{d'} \Sigma_{n,d,d'}(\pi_d \circ \mathbf{s}) (\pi_d \circ \mathbf{s})_{n,d',h}^v \\ &= \sum_{d'} \Sigma_{n,\pi_d(d),\pi_d(d')}(\mathbf{s}) \mathbf{s}_{n,\pi_d(d'),h}^v \\ &= \sum_{d'} \Sigma_{n,\pi_d(d),d'}(\mathbf{s}) \mathbf{s}_{n,d',h}^v = \pi_d \circ \text{Attn}_D(\mathbf{s}).\end{aligned}$$

This concludes the proof. \square

We continue by defining and proving the properties of the second main component of the bi-dimensional attention block: Attn_N .

Definition 7. Let $\text{Attn}_N : \mathbb{R}^{N \times D \times H} \rightarrow \mathbb{R}^{N \times D \times H}$ be a self-attention block [32] acting across N (i.e. the sequence length). Let σ be a softmax activation function operating on the last dimension of a tensor. Then Attn_N is defined as

$$\text{Attn}_N(\mathbf{s})[n, d, h] = \sum_{n'=1}^N \Sigma_{n,d,n'}(\mathbf{s}) \mathbf{s}_{n',d,h}^v, \text{ where } \Sigma_{n,d,n'}(\mathbf{s}) = \sigma\left(\frac{1}{\sqrt{H}} \sum_{\ell} \mathbf{s}_{n,d,\ell}^k \mathbf{s}_{n',d,\ell}^q\right)$$

given a linear projection of the inputs \mathbf{s} which maps them into keys (k), queries (q) and values (v)

$$\mathbf{s}_{n,d,\ell}^k = \sum_j \mathbf{s}_{n,d,j} \mathbf{W}_{j,\ell}^k, \quad \mathbf{s}_{n',d,\ell}^q = \sum_j \mathbf{s}_{n',d,j} \mathbf{W}_{j,\ell}^q, \quad \mathbf{s}_{n',d,h}^v = \sum_j \mathbf{s}_{n',d,j} \mathbf{W}_{j,\ell}^v.$$

Proposition 4. Attn_N is equivariant to Π_N and Π_D (i.e., across sequence length and input dimensionality).

Proof. Follows directly from proposition 3 after transposing the first and second dimension of the input. \square

Finally, we have the necessary ingredients to prove propositions 1 and 2 from the main paper.

Proposition 5. The bi-dimensional attention block \mathbf{A}_t is equivariant to Π_D and Π_N .

Proof. The bi-dimensional attention block simply adds the output of Attn_D and Attn_N , followed by an element-wise non-linearity. Therefore, as a direct application of lemma 2 the complete bi-dimensional attention block remains equivariant to Π_N and Π_D . \square

C.3 NDP Noise model

By building on the equivariant properties of the bi-dimensional attention block, we prove the equivariance and invariance of the NDP's noise models, denoted by ϵ_θ^x and ϵ_θ^y , respectively. We refer to fig. C.1 for their definition. In short, ϵ_θ^x consists of adding the output of several bi-dimensional attention blocks followed by dense layers operating on the last dimension. Similarly, ϵ_θ^y is constructed by summing the bi-dimensional attention blocks, but is followed by a summation over D before applying a final dense layer.

The following propositions hold:

Proposition 6. *The function ϵ_θ^x is equivariant to Π_D and Π_N .*

Proof. The output ϵ_θ^x is formed by element-wise summing the output of bi-dimensional attention layers. Directly applying lemma 1 and proposition 5 completes the proof. \square

Proposition 7. *The function ϵ_θ^y is equivariant to Π_N .*

Proof. The summation over D does not affect the equivariance over Π_N from the bi-dimensional attention blocks as it can be cast as a row-wise operation. \square

Proposition 8. *The function ϵ_θ^y is invariant to Π_D .*

Proof. Follows from the equivariance of the bi-dimensional blocks and Theorem 7 from Zaheer et al. [35]. \square

D Additional Information on the Experiments

D.1 Experimental setup

Here we provide more detailed information describing how the numerical experiments were conducted.

All experiments share the same model architecture illustrated in Figure 1, there are however a number of model parameters that must be chosen. An L1 (i.e., Mean Absolute Error, MAE) loss function was used throughout. We use five bi-dimensional attention blocks, each consisting of multi-head self-attention blocks [32] containing a representation dimensionality of $H = 64$ and 8 heads. Each experiment used either 500 or 1,000 diffusion steps, where we find larger values produce more accurate samples at the expense of computation time. Following Nichol et al. [20] we use a cosine-based scheduling of β_t during training. The Adam optimiser is used throughout. Our learning rate follows a cosine-decay function, with a 20 epochs linear learning rate warm-up to a maximum learning rate of $\eta = 0.001$ before decaying. All NDP models were trained for 250 epochs with the exception of the lengthscale marginalisation experiment, which was trained for 500 epochs. Each epoch contained 4096 example training $(\mathbf{y}_0, \mathbf{x}_0)$ pairs. Training data was provided in batches of 32, with each batch containing data with the same kernel hyperparameters but different realisations of prior GP samples. The complete configuration for each experiment is given in table 1

Experiments were conducted on a 32-core machine and utilised a single Tesla V100-PCIE-32GB GPU. Training of each model used in the experiments takes no longer than 30 minutes.

Table 1: Experiment configuration and training time. Bold values indicate a deviation from the fiducial values used in the regression experiments.

Experiment	1D regression	Hyperparameter marginalisation	2D regression	High dim BO	1D opt
Epochs	250	500	250	250	250
Total samples seen	1024k	2048k	1024k	1024k	1024k
Batch size	32	32	32	32	32
Loss	L1	L1	L1	L1	L1
LR decay	cosine	cosine	cosine	cosine	cosine
LR init	0.001	0.001	0.001	0.001	0.001
LR warmup epochs	20	20	20	20	20
Num blocks	5	5	5	5	5
Representation dim (H)	64	64	64	64	64
Num heads	8	8	8	8	8
Num timesteps (T)	500	1000	500	500	2000
Num data per batch (N)	100	100	100	256	100
Deterministic inputs	True	True	True	True	False
Training time (mins)	17	33	16	21	16

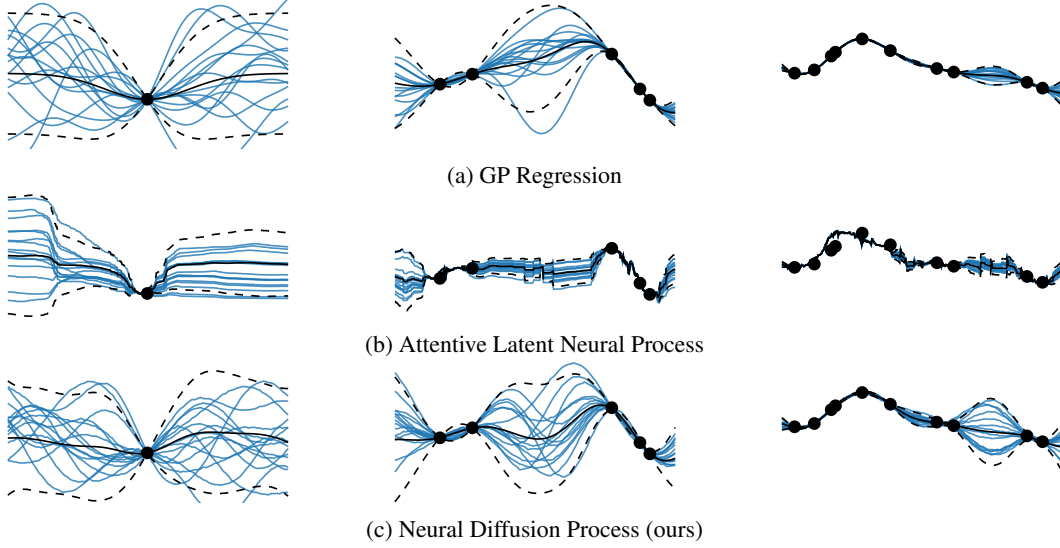


Figure D.1: **1D regression:** The blue curves are posterior samples from different probabilistic models. We also plot the empirical mean and two standard deviations of the samples in black. From left to right we increase the number of data points (black dots) and notice how the process gets closer to the true underlying function.

Time embedding The diffusion step t is a crucial input of the neural network noise estimator as the model needs to be able to differentiate between noise added at the start or the end of the process. Following Vaswani et al. [32] we use a cyclic 128-dimensional encoding vector for each step

$$t \mapsto [\sin(10^{\frac{0 \times 4}{63}} t), \sin(10^{\frac{1 \times 4}{63}} t), \dots, \sin(10^{\frac{64 \times 4}{63}} t), \cos(10^{\frac{0 \times 4}{63}} t), \dots, \cos(10^{\frac{64 \times 4}{63}} t)] \in \mathbb{R}^{128}$$

Data In our experiments, we provide training data to the models in the form of unique prior samples from a ground truth GP model. As specified in section 2 the input for each prior sample, \mathbf{x}_0 , may be randomly sampled or deterministically spaced across the relevant input range. For all but the last experiment we deterministically space \mathbf{x}_0 during training and inference in the hypercube $[-1, 1]^D$, where D is the dimensionality of the input. For $D \leq 2$ the spacing of points is a simple linear spacing (a grid for $D = 2$), in $D > 2$ we sample \mathbf{x}_0 according to a Halton sequence in the hypercube. The corresponding output \mathbf{y}_0 is sampled from a GP prior $\mathbf{y}_0 | \mathbf{x}_0 \sim \mathcal{N}(\mathbf{0}, k_\psi(\mathbf{x}_0, \mathbf{x}_0) + \sigma^2)$ where the kernel is a stationary kernel (Matern $\frac{3}{2}$, Matern $\frac{5}{2}$ or exponentiated quadratic, indicated in each experiment) with hyperparameters $\psi = [\ell, \sigma_k^2]$ corresponding to the automatic relevance determination (ARD) lengthscales and kernel variance respectively. Kernel hyperparameters are fixed for all experiments except for section 4 where we allow the model to observe data from a variety of different lengthscales during training. The noise variance is fixed to $\sigma^2 = 10^{-6}$ and the kernel variance is fixed to $\sigma_k^2 = 1.0$ throughout.

D.2 1D Conditional samples

In the experiment, we use GPflow [31] for the GP regression model using a kernel that matches the training data: a squared exponential with lengthscale set to 0.2. The other baseline, namely the Attentive Latent NP, is a pretrained model which was trained on a dataset with the same configuration. The ALNP model originates from the reference implementation of Dubois et al. [3]. Figure D.1 shows additional conditional samples.

D.3 High-dimensional BO

In this experiment, we perform Bayesian optimisation on the Hartmann 3D and 6D objectives. We re-scale, without loss of generality, the inputs of the objectives such that the search space is $[-1, 1]^D$ for both. We refer to <https://www.sfu.ca/~ssurjano/hart3.html> and <https://www.sfu.ca/~ssurjano/hart6.html> for more details about Hartmann 3D and 6D, respectively.

The baseline models, GPR and Random, originate from Trieste [1] — a TensorFlow/GPflow based Bayesian Optimisation Python package. We compare them against two NDP models: Fixed and Marginalised. The Fixed NDP model is trained on Matérn-5/2 samples with a fixed lengthscale set to 0.5 along all dimensions. The Marginalised NDP model is trained on Matérn-5/2 samples originating from different lengthscales, where the lengthscales are drawn from a log-Normal prior $\log \mathcal{N}(0, 1)$.

D.4 Optimisation using density estimation

In the last experiment, we present a novel global optimisation scheme which relies on input density estimation. For a given target observation value y^* we use the NDP’s ability to sample from $p(x^* | y^*, \mathcal{D})$ to obtain a new query point. The target value y^* is estimated from the current dataset. For the experiment, we sample y^* from a half-normal, where the mean corresponds to the minimum of the observed function values, the variance corresponds to the variance of the observations, and domain is between the minimum and $-\infty$.

E Code

The code is available at <https://github.com/vdutor/neural-diffusion-processes>.

Preprocessing method

The NDP’s noise model starts by rearranging the inputs $x_t \in \mathbb{R}^{N \times D}$ and $y_t \in \mathbb{R}^N$ to be of shape $[N, D, 2]$, as explained in section 3.1 and shown in the red box in fig. C.1. Below we show the code which is responsible for this preprocessing:

```
import tensorflow as tf

def preprocess(x: tf.Tensor, y: tf.Tensor) -> tf.Tensor:
    """
    Transform inputs to split out the x dimensions for dimension-
    agnostic processing.

    :param x: [B, N, D]
    :param y: [B, N, 1]
    :return: [B, N, D, 2]
    """
    D = tf.shape(x)[-1]
    x = tf.expand_dims(x, axis=-1)
    y = tf.repeat(tf.expand_dims(y, axis=-1), D, axis=2)
    return tf.concat([x, y], axis=-1)
```